Aerosol and Air Quality Research

ORIGINAL RESEARCH
https://doi.org/10.4209/aaqr.210201

Porous Zeolitic Imidazolate Framework Loaded Mn as an Efficient Catalyst for the Selective Catalytic Reduction of NO_x with NH_3

Yongliang Chen[1], Meiqing Yu[1,2], Rui Wang[1*]

[1] School of Environmental Science and Engineering, Shandong University, Jimo, Qingdao 266237, China
[2] Undergraduate School, Shandong University, Jinan 250199, China

ABSTRACT

Zinc 2-methylimidazolate ($Zn(Me\text{-}Im)_2$, ZIF-8) was synthesized through solvothermal method, and the Mn@ZIF-8 was synthesized by loading the Mn species onto the prepared ZIF-8 through impregnation. The effect of the addition amount of Mn species on the activity in selective catalytic reduction of NO_x with NH_3 (NH_3-SCR), the stability of catalysts at ideal temperatures and the resistance to H_2O and SO_2 were investigated. Moreover, the characterizations of the catalysts including XRD, SEM, EDS, XPS, BET, TGA and H_2-TPR were carried out. The results indicated that SCR activity of the catalysts was related to the addition amount of Mn species, the Mn@ZIF-8(0.8) showed the best NO conversion of over 90% ranging from 225°C–400°C with good stability in a long-time test. Besides, the Mn@ZIF-8 showed a high resistance to SO_2. The ZIF-8 has a great potential to be an excellent support, and Mn@ZIF-8 is promising catalyst in SCR reaction.

Keywords: Nitrogen oxides, SCR, Zeolitic imidazolate framework, ZIF-8

1 INTRODUCTION

Nitrogen oxides (NO_x), mainly NO and NO_2, is a kind of common gaseous pollutant, and the removal of NO_x has long been a difficult problem in air pollution control. The sources of NO_x can be divided into two categories, one is the mobile sources and the other is the fixed sources. The fixed sources mainly refer to the flue gas emitted from the combustion of fossil fuels such as coal and oil in the process of industrial production, and the mobile sources are generally thought to be the exhaust gas emitted from automobile engine. With the rapid development of modern industrialization, a large amount of fossil fuels have been exploited and consumed, making the NO_x emitted into the atmosphere far exceed the carrying capacity and self-purification capacity of the atmospheric environment. NO_x brought severe harm to environment, such as the photochemical smog, acid rain and ozone holes. All these environmental pollution phenomena are related to the emission of NO_x, and have a serious threat to our human beings. Consequently, it is essential to control the NO_x in the atmosphere (Brandenberger *et al.*, 2008; Busca *et al.*, 2008; Forzatti, 2001; Twigg, 2007).

NH_3-SCR has been proven to be the most effective technique for abatement of NO_x (Chen *et al.*, 2016). And the catalyst with high denitrification efficiency is the key of the SCR technique. So far, the SCR catalysts can be divided into the following categories according to their active components: noble metal catalysts (Li *et al.*, 2010; Qi *et al.*, 2004), metal oxides catalysts (Qi *et al.*, 2003a; Wei *et al.*, 2018; Shen *et al.*, 2016) and molecular sieve catalysts (Brandenberger *et al.*, 2008; Delahay *et al.*, 2005; Gao *et al.*, 2017). Though the commercial catalysts V_2O_5-$WO_3(MoO_3)/TiO_2$ have been widely used, the defects like narrow temperature window and toxicity of vanadium pentoxide still exist (Yi *et al.*, 2016). Hence, the novel catalysts with wide temperature window and environment-friendly properties is desirable.

OPEN ACCESS

Received: August 14, 2021
Revised: September 10, 2021
Accepted: September 14, 2021

* **Corresponding Author:**
wangrui@sdu.edu.cn

Publisher:
Taiwan Association for Aerosol Research
ISSN: 1680-8584 print
ISSN: 2071-1409 online

Manganese oxide (MnO_x), a kind of transition metal oxide, has attracted great attentions due to its various labile oxygen species and high activity in NH_3-SCR reaction (Wu *et al.*, 2007). Min *et al.* (2007) prepared different types of MnO_x catalysts through a precipitation method, and got a high NO_x conversion for the SCR of NO_x with NH_3. To enhance the performance of MnO_x catalyst, a series of doping species and supporter was applied. Peng *et al.* (2016) used Eu to modify MnO_x catalyst to promote SCR activity, and the results showed that $MnEuO_x$ exhibited a high NO_x conversion in a wide temperature range of 150–400°C. CeO_2 was a another metal species used to improve the SCR activity of MnO_x. Qi *et al.* (2003b, 2004) prepared mixed manganese and cerium oxides, and the MnO_x-CeO_2 was highly active in SCR reaction obtaining almost 95% NO conversion at 150°C. Singoredjo *et al.* (2010) prepared the alumina supported MnO_x exhibiting a high NO_x conversion during 120–300°C. TiO_2 is another kind of support commonly used to facilitate the SCR activity of MnO_x, Park *et al.* (2013) loaded Mn on synthesized TiO_2 through impregnation method, exhibiting a high NO conversion of almost 100% at 150°C. Besides, a series of metal species such as Fe, Ce, V, Sm, Zr, were used to modify the MnO_x/TiO_2 to avoid poor resistance to SO_2 of MnO_x. Yet, the result could not meet the requirements of industrialization, further investigation is still needed (Yang *et al.*, 2016; Niu *et al.*, 2016; Zhang *et al.*, 2018; Sun *et al.*, 2018).

Metal organic frameworks (MOFs), the porous crystalline materials, have drawn extensive research interests due to their higher specific surface area, higher porosity, and more stable porous structure compared to the metal oxides (Lee *et al.*, 2009). It is advantageous for them to adsorb the reactants and provide great gas storage, separation and catalysis, besides, the high specific surface, well ordered porous structure, and regular crystal structure have proven the MOFs to be ideal support (Zhang *et al*., 2016; Wang *et al.*, 2016; Zhang *et al.*, 2017). Zhang *et al.* (2017) loaded Mn and Ce onto MOFs through in situ and impregnation methods, and studied their catalytic activities in SCR reaction, the results showed that MnCe@MOF had a high NO_x conversion in a wide temperature range. Wang *et al.* (2016) prepared the CeO_2/MIL-100(Fe) catalysts by encapsulating ceria nanoparticles into MIL-100(Fe) through impregnation, the CeO_2/MIL-100(Fe) catalyst showed a high NH_3-SCR activity and great resistance to SO_2 at 196–300°C. Zeolitic imidazolate framework (ZIFs), a sort of MOFs, has higher specific surface area and better thermal stability than ordinary MOFs (Huang *et al.*, 2010; Park *et al.*, 2006). Among them, ZIF-8 is the most widely studied ZIFs with a specific surface area of 1400 $m^2\ g^{-1}$ and great thermal stability (Park *et al.*, 2006; Venna *et al.*, 2010), and has been widely used in gas adsorption, hydrogen storage and catalysis. However, few researchers have applied ZIF-8 in NH_3-SCR reaction (Banerjee *et al.*, 2008; Küsgens *et al.*, 2009; Nguyen *et al.*, 2012).

In this work, ZIF-8 was synthesized through a solvothermal method, and MnO_x was firstly loaded on ZIF-8 by impregnation. The activity of the catalysts in NH_3-SCR reaction, the stability of the catalysts, the effect of the addition amount of Mn species on catalytic activity as well as the resistance to H_2O and SO_2 were investigated. Besides, the characterization of the catalysts including XRD, SEM, EDS Mapping, XPS, BET, and H_2-TPR, TGA was carried out to research the catalysts for further information.

2 EXPERIMENTAL

2.1 Materials

All the chemicals were available commercially and used without further purification. 2-methylimidazole (2-HMeIM, 99%) Zinc nitrate Hexahydrate ($Zn(NO_3)_2{\cdot}6H_2O$, 99%) were purchased from Tianjin Kemiou Chemical Reagent Co., Ltd. N,N-Dimethylformamide (DMF 99.5%) and 50% Manganese nitrate water solution ($Mn(NO_3)_2$ 50%) were purchased from Tianjin Fuchen Chemical reagents factory.

2.2 Synthesis of Catalyst

2.2.1 Synthesis of ZIF-8 particles

ZIF-8 was synthesized by solvothermal method according to the following procedure (Gee *et al.*, 2013; Tran *et al.*, 2011): A solid mixture of $Zn(NO_3)_2{\cdot}6H_2O$ (0.717 g, 2.41 mmol) and 2-methylimidazole (H-MeIM) (0.18 g, 2.19 mmol) was dissolved in 50 mL DMF, the solution was

transferred into a teflon-line stainless steel autoclave, and heated to 140°C at a rate of 5°C min^{-1} in a temperature-programmed oven and maintained for 24 h. After cooling to ambient temperature, the crystal was collected and washed with DMF for three times. Finally, these samples were dried at 60°C overnight to remove the residual solvents.

2.2.2 Synthesis of Mn@ZIF-8

The Mn was loaded on ZIF-8 via impregnation method reported by Zhang *et al.* (2017). Adding 0.4, 0.6, 0.8, and 1 mL of $Mn(NO_3)_2$ respectively into 20 mL methanol to get Mn solutions, and dispersing 1 g of ZIF-8 into 30 mL methanol under ultrasonication for 15 min to get a ZIF-8 solution. Then, the Mn solution was slowly dropped into ZIF-8 solution under vigorous stirring for 4 h, followed by filtration to get the precipitate, after that, the precipitate was dried overnight at 60°C. Finally, the precipitate was heated at 300°C for 5 h. The obtained samples were denoted as Mn@ZIF-8(0.4), Mn@ZIF-8(0.6), Mn@ZIF-8(0.8) and Mn@ZIF-8(1), respectively. For convenience, the Mn@ZIF-8 without note represents the Mn@ZIF-8(0.8).

2.3 Characterizations of the Catalysts

The XRD patterns were obtained on a Bruker D8 diffractometer using Cu Kα radiation between 2θ = 5° and 45°. The micro-morphology of Mn@ZIF-8 was investigated by scanning electron microscope (SEM) (SU 8010), and energy dispersive spectroscopy (EDS) mapping images were obtained on the same device. The X-ray photoelectron spectroscopy (XPS) analysis was carried on a Thermo Fisher Scientific ESCALAB 250 spectrometer, the correction of binding energy shift was referenced to C 1s line at 284.6 eV, and the spectra of the Mn 2p and O 1s were recorded. The specific surface area analysis was conducted on Micromeritics Tri StarII 3020 Surface Arae and Porosity Analyzer with a N_2 adsorption, and the results were calculated with the multi-point Brunauer-Emmett-Teller (BET) approach. The thermogravimetric analysis (TGA) was carried on a TGA SDT Q600 thermogravimetric analyzer with a heating rate of 10°C min^{-1} from 25°C to 600°C under nitrogen atmosphere. The hydrogen temperature programmed reduction (H_2-TPR) analysis was performed in which 100 mg of the samples were preheated to 450°C with a ramp rate of 10°C min^{-1} under N_2 atmosphere. After cooling to the ambient temperature, the samples were heated up to 800°C at a ramp rate of 8°C min^{-1} with a flow of H_2, and the consumption of H_2 was continuously recorded using the TCD detector.

2.4 Activity Tests

The tests of NH_3-SCR activity were carried out in a fix-bed quartz reactor (8 mm in diameter) heated by a tube furnace. The simulated flue gas contained 500 ppm NO, 500 ppm NH_3, 5% O_2, 3% H_2O (when used), 200 ppm SO_2 (when used) and balance N_2, which were regulated by mass flow controllers respectively. In each run of SCR test, 0.2 g of Mn@ZIF-8 was used and the total flow rate was controlled at 100 mL min^{-1} corresponding to a gas hourly space velocity (GHSV) of approximately 240000 h^{-1}. The catalyst was heated to the temperature ranging from 100°C to 450°C at a rate of 10°C min^{-1}, and held at each temperature spots for 50 min. Concentrations of NO and NO_2 were simultaneously monitored by the NO and NO_2 analyzers (TH-9905), and N_2O in the outlet gas was measured by an Antaris™ IGS Gas Analyzer from Thermo Fisher Scientific Inc. The NO_x conversion rate and the N_2 selectivity were calculated as follows:

$$NO_x \text{ conversion } (\%) = \left(1 - \frac{[NO_x]_{out}}{[NO_x]_{in}}\right) \times 100\%, \quad (1)$$

$$N_2 \text{ selectivity } (\%) = \left(1 - \frac{2[N_2O]_{out}}{[NO_x]_{in} + [NH_3]_{in} - [NO_x]_{out} - [NH_3]_{out}}\right) \times 100\% \quad (2)$$

where the subscripts “in” and “out” refers to the inlet concentration and outlet concentration at steady state, respectively.

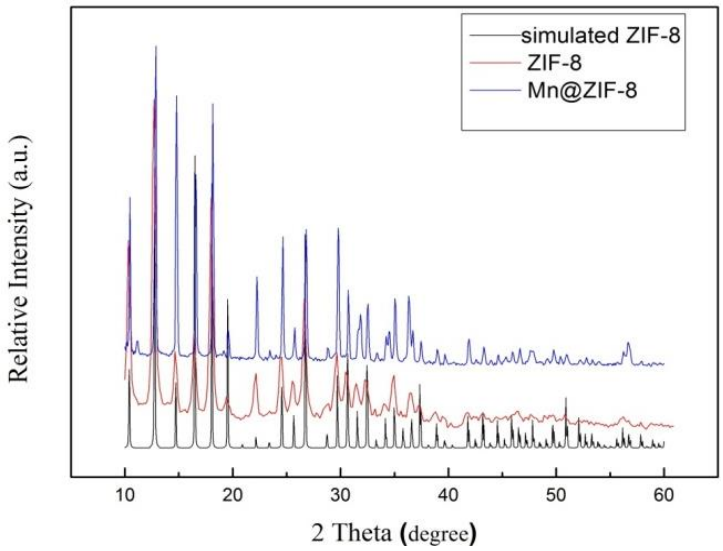

Fig. 1. XRD patterns of the catalysts.

3 RESULTS AND DISCUSSION

3.1 Characterizations of the Catalysts

3.1.1 XRD

To determine the crystal structure of the catalysts, the XRD analysis of the synthesized ZIF-8 and Mn@ZIF-8 was carried out. It could be easily seen from Fig. 1 that the characteristic peak of synthesized ZIF-8 was in accordance with the simulated ZIF-8, which approved the ZIF-8 was successfully synthesized. As for the XRD pattern of Mn@ZIF-8, no apparent difference was found after the impregnation, indicating that the crystalline structure of ZIF-8 retained well. Yet, the characteristic peaks of Mn species were not observed which may be interpreted by that the Mn species were in amorphous phase (Li *et al.*, 2017).

3.1.2 SEM and EDS Mapping

SEM was carried to investigate the structure of Mn@ZIF-8. It can be seen from Fig. 2 that the synthesized catalysts still retained its dodecahedral shape, which matched well with the results of XRD analysis. Moreover, EDS Mapping was performed to demonstrate the distribution of Mn, Zn species, and it could be seen that the elements of Mn and Zn are uniformly distributed on the whole surface of the catalysts, which was beneficial for adsorption and activation of the reactants, and was conducive to the NH_3-SCR catalytic activity.

3.1.3 XPS spectra

To further investigate the chemical state of Mn elements in the catalysts, XPS spectra were recorded and displayed in Fig. 3(a), from which it could be seen obviously that two prominent peaks at 642.89, 654.73 eV accompanied by two satellite peaks at 641.53, 653.46 eV were gained after fitting by Gaussian components. The peaks at 641.53 eV, 653.46 eV could be attributed to Mn^{2+} species, while the peaks at 642.89 eV and 654.73eV could be assigned to Mn^{3+} (Becerra *et al.*, 2011; Guo *et al.*, 2016). According to previous reports, the co-existence of Mn^{2+} and Mn^{3+} on the catalysts could facilitate the formation of oxygen vacancies, which played an important role in low temperature oxidation property (Liu *et al.*, 2012). Besides, the high valence state of Mn^{3+} species would improve the reducibility of the sample (Cheng *et al.*, 2017).

The O 1s XPS spectra of the Mn@ZIF-8 were shown in Fig. 3(b), two asymmetric peaks could be observed, indicating there were two distinct types of oxygen species. The lower binding energy peak at 530.27 eV was ascribed to the lattice oxygen species O^{2-} in the catalysts, and the sub-bands at 531.71 ev was attributed to surface chemisorbed oxygen species, such as O^{2-} or O^{-} (Atribak *et al.*, 2011).

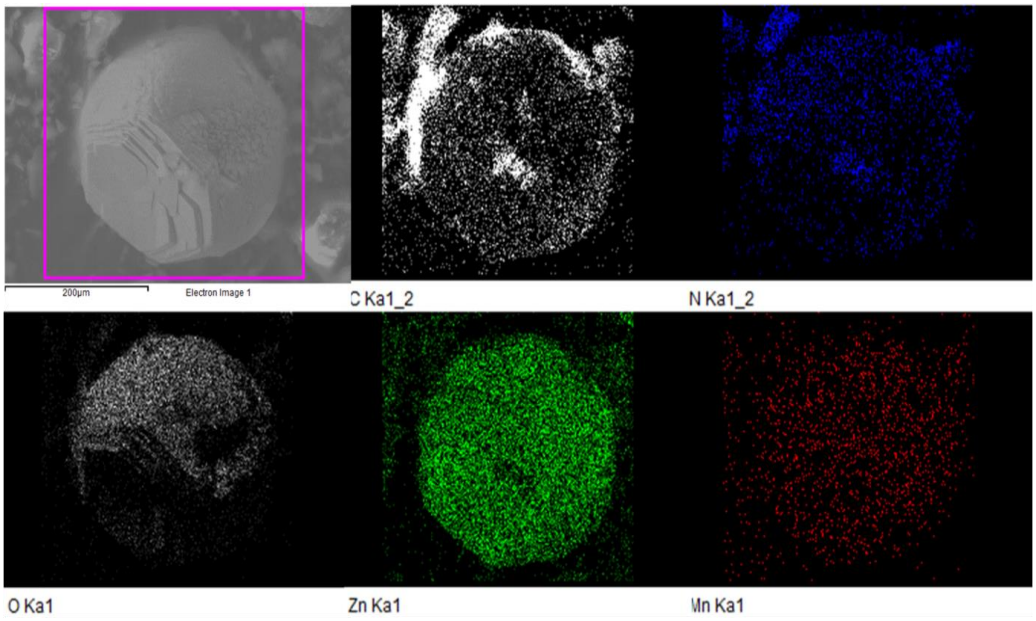

Fig. 2. SEM image and EDS Mapping of Mn@ZIF-8.

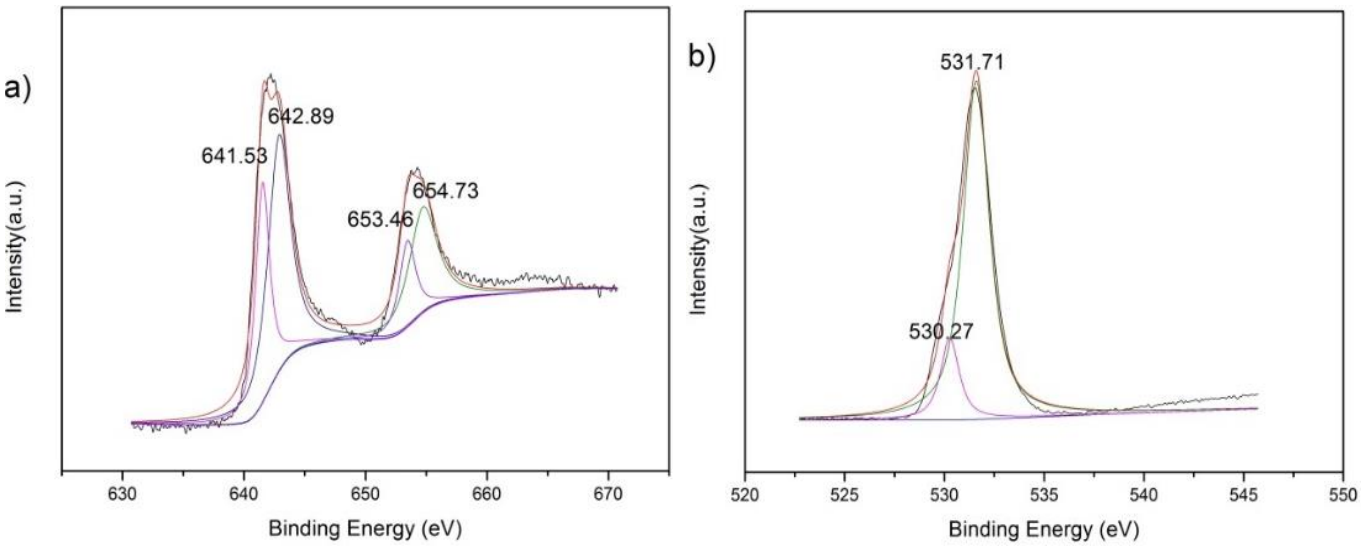

Fig. 3. XPS spectra of (a) Mn 2p and (b) O 1s for Mn@ZIF-8.

3.1.4 H_2-TPR

To investigate the redox behavior of Mn@ZIF-8, the H_2-TPR analysis was performed, and the results were presented in Fig. 4, from which it could be seen that there are two main reduction peaks. The first peak located at around 250°C could be assigned to the reduction of MnO_2 to Mn_2O_3 and the following peak around 520°C could be attributed to the further reduction of Mn_2O_3 to MnO (Zhao *et al.*, 2016; Du *et al.*, 2018). Normally, the operational temperature should be lower than 450°C. This prominent peak could be caused by the reduction of $Mn^{3+} \rightarrow Mn^{2+}$and the decomposition of ZIFs based on the TGA curves. Then, it could be speculated that the doping of Mn species prompted the catalysts to have the stronger redox behavior and oxygen storage capacity of the catalyst, which played an important role in the SCR activities (Li *et al.*, 2016).

3.1.5 BET analysis

The BET surface area of a catalyst support plays a significant role in the NH_3-SCR reaction. Besides, the high BET surface area of the support can improve the catalytic activity considerably

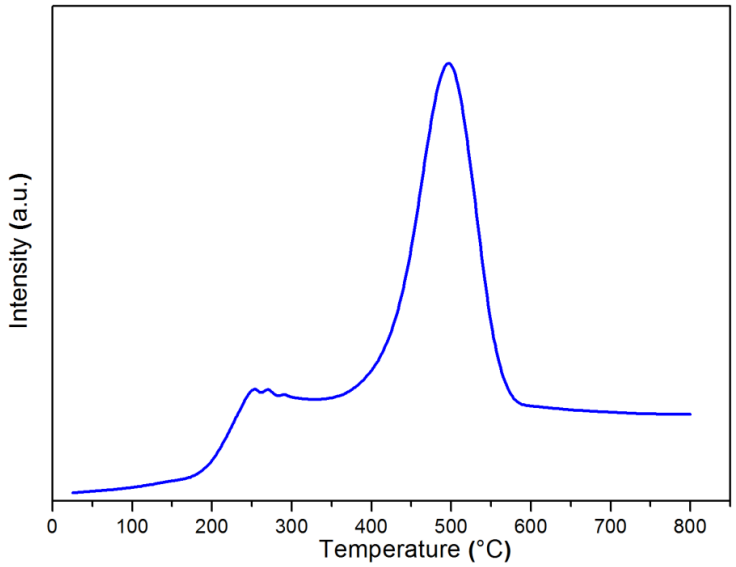

Fig. 4. H_2-TPR profiles of the catalysts.

Table 1. BET surface area of the catalysts.

Catalysts	BET surface area ($m^2\ g^{-1}$)
ZIF-8	1380.73
0.4Mn@ZIF-8	1623.26
0.6Mn@ZIF-8	1758.19
0.8 Mn@ZIF-8	1911.34
1 Mn@ZIF-8	1689.17

by means of enhancing the dispersion of active components to avoid aggregation, as well as the transfer of charge (Han *et al.*, 2015; Wang *et al.*, 2013). The BET surface areas of all the samples were listed in Table 1. It can be seen that the high surface area of ZIF-8 would be beneficial to the high NO_x conversion and the surface area of the samples was increased with the increase of the addition of Mn species, however, when the addition amount of Mn species reached 1 mL (in $Mn(NO_3)_2$ solution volume), the surface area began to decline. The decrease in specific surface area may be due to the excessive Mn loading caused formation of large solids and pores clogging of the ZIFs materials. The variation trend of the surface area was in accordance with the SCR activities, which indicated that the BET surface area was an important factor that influenced the SCR activities of the samples.

3.1.6 Thermogravimetric analysis of Mn@ZIF-8

As was well known, the MOFs usually have relatively poor thermal stability, yet, the thermal stability of the catalysts has a great impact on the SCR reaction. To investigate the stability of Mn@ZIF-8, the thermal gravimetric analysis was conducted, and the result shown in Fig. 5 exhibited a slightly weight loss of 5% from room temperature to 450°C, corresponding to the depletion of guest molecules, mainly H_2O, indicating the structure of Mn@ZIF-8 maintained well under 450°C, and Mn@ZIF-8 has a high thermal stability. When the temperature was higher than 450°C, a sharp weight loss of the sample appeared, which could be ascribed to the oxidation of organic ligands and the collapse of the structure of Mn@ZIF-8, which may account for the decrease in activity of the catalysts.

3.2 The Effect of Loading Amount of Mn Species

The NO_x conversion of all the catalysts in the range of 200–450°C was shown in Fig. 6, from which it could be seen that more Mn species leaded to higher catalytic activity of the samples till the Mn@MOF(0.8) which presented the highest deNO_x efficiency compared with the rest

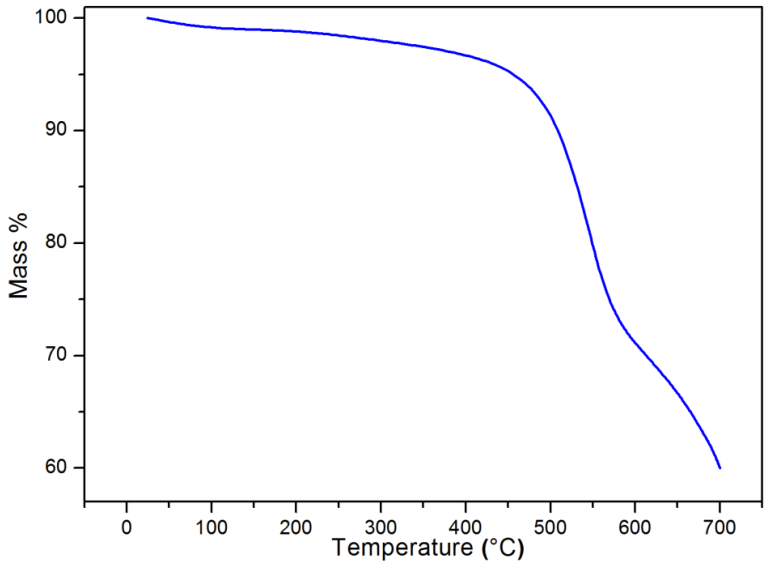

Fig. 5. The TGA curves obtained for the Mn@ZIF-8.

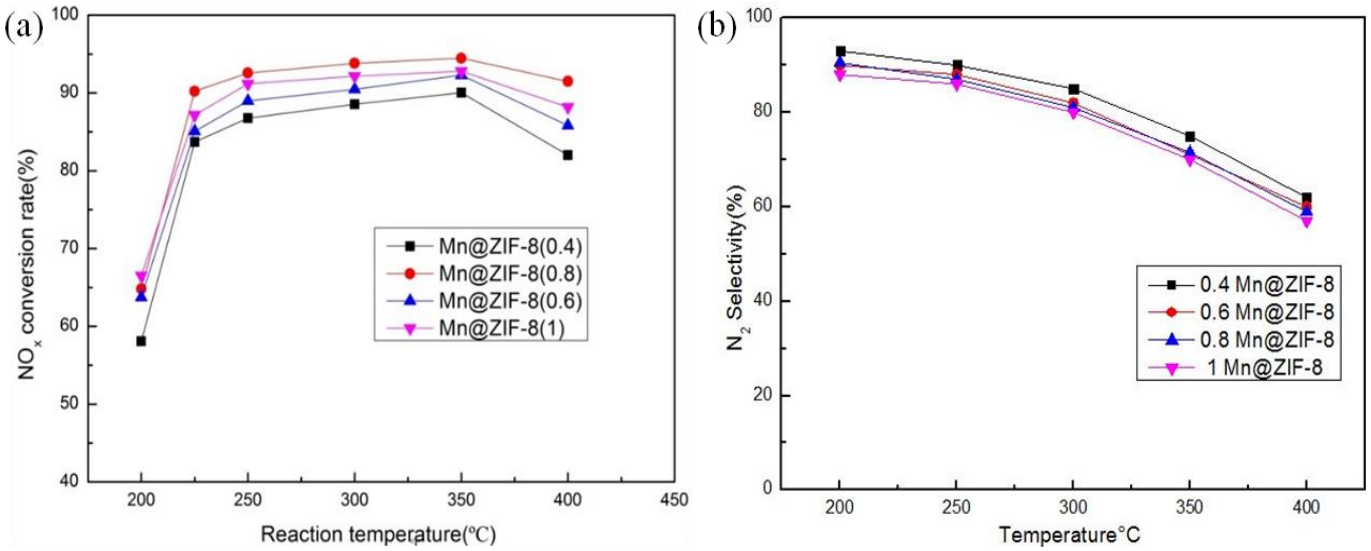

Fig. 6. (a) Catalytic SCR activities and (b) N_2 selectivity of the catalysts. Reaction conditions: [NH_3] =500 ppm, [NO] =500 ppm, [O_2] = 3%, N_2 = balance and total flow rate =100 mL min^{-1}.

Mn loadings. The NO_x conversion of Mn@ZIF-8(0.8) was over 90% in the range of 225–400°C, and reached 100% at 350°C. However, when the loading amount of Mn species exceeded 1 mL (in $Mn(NO_3)_2$ solution volume), the catalytic activity began to decline, which may be caused by the severe decrease of BET surface area. On the other hand, the NO_x conversion of all the samples increased with the rising of temperature within 200–350°C, and when the temperature went up to 400°C, the NO_x conversion began to decrease, which may be inferred from the TGA analysis that this decreased activity may be caused by the collapse of ZIF-8 framework.

N_2O is also an important pollutant in the air. Using traditional Mn-based catalysts, a large amount of N_2O was produced by side reaction and therefore limited its application. In view of this, the formation of N_2O in the SCR reaction was tested, and the N_2 selectivity of catalysts with different loadings was studied. As shown in Fig. 6(b), the N_2O was formed in all catalysts. With the increase of temperature, ammonia was oxidized to N_2O gradually, and the nitrogen selectivity of the catalyst decreased continuously. Besides, the nitrogen selectivity of the catalyst decreased when the loading amount of Mn species increased. Yet the nitrogen selectivity was still over 70% with higher catalyst activity in the temperature window of 250–350°C.

3.3 Stability Test of Mn@ZIF-8

Besides, the stability tests of the catalysts at 350°C was carried out, and as illustrated in Fig. 7, the NO_x conversion of Mn@ZIF-8 maintained high level after 12 h, presenting a good stability under the identical temperature, which may be ascribed to the porous structures of ZIF-8 and the strong interaction between Mn species and ZIF-8 (Zhang *et al.*, 2014).

3.4 Effect of SO_2 and H_2O on Mn@ZIF-8

As the existence of H_2O and SO_2 is unavoidable in the exhaust, even after desulfurization, the residual H_2O and SO_2 still exert a notable impact on SCR performance. Therefore, the effects of SO_2 and H_2O on the NO_x conversion of Mn@ZIF-8 were investigated. The results shown in Fig. 8 revealed that the NO_x conversion decreased slightly after introducing 200 ppm of SO_2, and then reached a relatively steady state. After cutting off the input of SO_2, the conversion of NO_x was gradually restored its original level and remained stable. Hence, it could be concluded that the Mn@ZIF-8 had a great resistance to SO_2, and the process of SO_2 inhibition is reversible. Besides, the negative effect of SO_2 on SCR reaction could be attributed to the following aspects: on one hand, the SO_2 would compete with the reactants for the active sites, on the other hand, the formed sulfate depositing (ammonium sulfate and ammonium bisulfate species) would block the active sites (Lu *et al.*, 2015). Yu *et al.* (2010) proposed that the porous structure was in favor of the great SO_2 resistance. The high sulfur resistance of Mn based catalysts was related to porous silica support (Huang *et al.*, 2008). Thus, it could be inferred that the great SO_2 resistance of Mn@ZIF-8 may be ascribed to the porous structure of ZIF-8.

The impact of H_2O and SO_2 was also investigated. The NO_x conversion decreased to 65% under the coexistence of H_2O and SO_2 and could not recover to the original value after eliminating the SO_2+H_2O feeding as shown in Fig. 9, which demonstrated that there was a synergistic inhibition effect between H_2O and SO_2, and massive sulfate species and deposition were formed and blocked the active sites.

4 CONCLUSIONS

The XRD patterns and SEM image demonstrated that the Mn@ZIF-8 was synthesized successfully, and the Mn species were highly dispersed on ZIF-8. The Mn 2p XPS spectra proved that the Mn^{2+} and Mn^{3+} coexisted on the catalysts and played an important role in redox process.

The prepared Mn@ZIF-8 showed an over 90% NO conversion at the temperatures ranging from 225–400°C, the excellent catalytic activity may attributed to the huge specific surface area of ZIF-8,

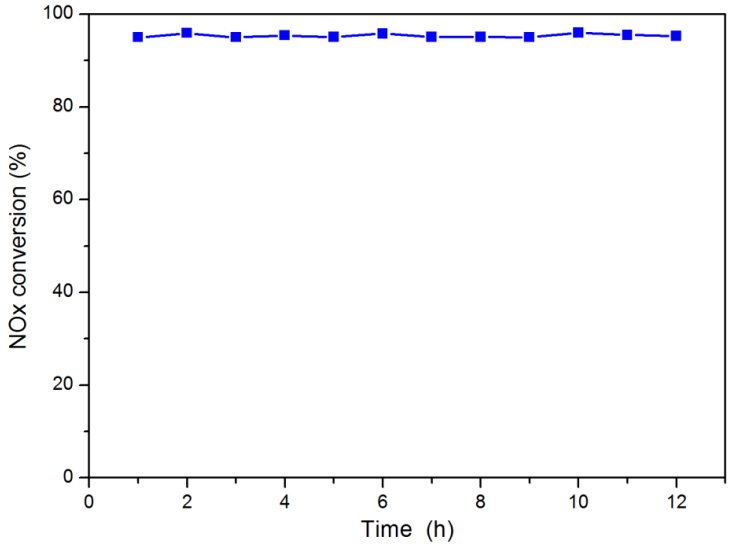

Fig. 7. The catalytic activity of Mn@ZIF-8. Reaction conditions: [NH_3] =500 ppm, [NO] =500 ppm, [O_2] = 5%, N_2 = balance and total flowrate =100 mL min^{-1}, T = 350°C.

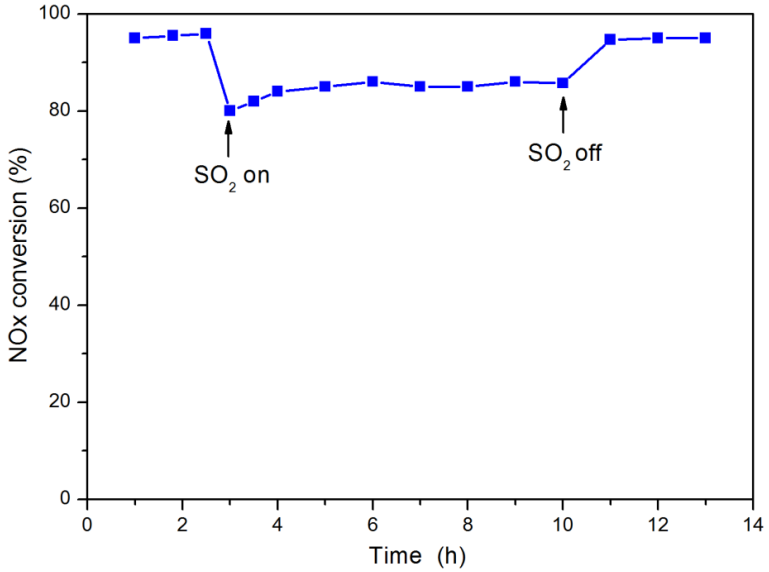

Fig. 8. The effect of SO_2 on the SCR activities of Mn@ZIF-8. Reaction conditions: [NH_3] = 500 ppm, [NO] = 500 ppm, [SO_2] =200 ppm, [O_2] = 5%, N_2 = balance and total flowrate =100 mL min^{-1}, T = 350°C.

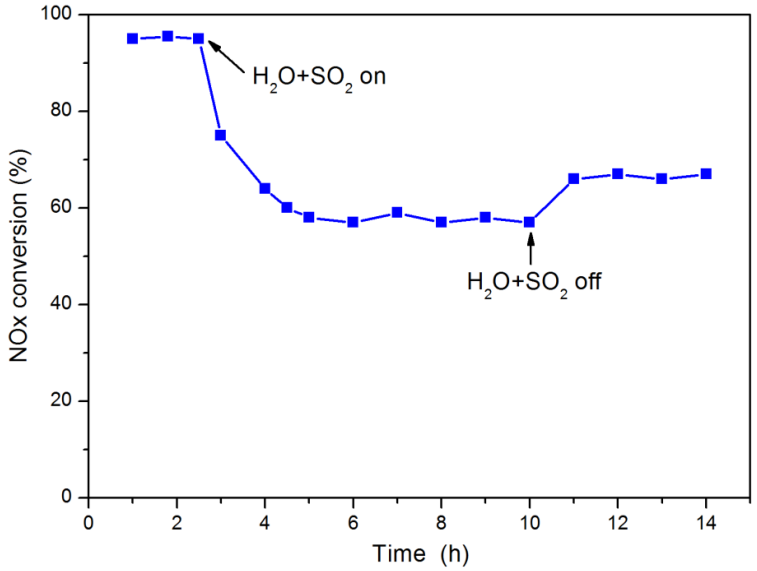

Fig. 9. The effect of SO_2 and H_2O on the SCR activities of Mn@ZIF-8. Reaction conditions: [NH_3] = 500 ppm, [NO] = 500 ppm, [SO_2] = 500 ppm, [O_2] = 5%, [H_2O] = 3%, N_2 = balance and total flowrate = 100 mL min^{-1}, T = 350°C.

as the variation trend of the surface area was in accordance with the SCR activities. Besides, the activity and stability for Mn@ZIF-8 was proved to be ideal after 12 h. Furthermore, the Mn@ZIF-8 exhibited strong tolerance against SO_2, which may be ascribed to the porous structure of ZIF-8. It is noteworthy that the catalytic activity of Mn@ZIF-8 was inhibited considerably in the presence of H_2O and SO_2. As a whole, this study demonstrated that the ZIF-8 is a kind of promising support and the use of Mn@ZIF-8 as a novel catalyst for SCR reaction is feasible.

CONFLICTS OF INTEREST

There are no conflicts to declare.

ACKNOWLEDGEMENTS

We would like to extend our sincere appreciation to the support from the National Natural Science Foundation of China (22078176).

REFERENCE

Atribak, I., López-Suárez, F.E., Bueno-López, A., García-García, A. (2011). New insights into the performance of ceria-zirconia mixed oxides as soot combustion catalysts. Identification of the role of "active oxygen" production. Catal. Today 176, 404–408. https://doi.org/10.1016/j.cattod.2010.11.023

Banerjee, R., Phan, A., Wang, B., Knobler, C., Furukawa, H., O'Keeffe, M. (2008). High-throughput synthesis of zeolitic imidazolate frameworks and application to CO_2 capture. Science 319, 939–943. https://doi.org/ 10.1126/science.1152516

Becerra, M.E., Arias, N.P., Giraldo, O.H., Suárez, F.E.L., Gómez, M.J.I., López, A.B. (2011). Soot combustion manganese catalysts prepared by thermal decomposition of $KMnO_4$. Appl. Catal., B 102, 260–266. https://doi.org/10.1016/j.apcatb.2010.12.006

Brandenberger, S., Kröcher, O., Tissler, A. (2008). The state of the art in selective catalytic reduction of NO_x by ammonia using metal-exchanged zeolite catalysts. Catal. Rev. Sci. Eng. 50, 492–531. https://doi.org/10.1080/01614940802480122

Busca, G., Lietti, L., Ramis, G., Berti, F. (2008). Chemical and mechanistic aspects of the selective catalytic reduction of NO_x by ammonia over oxide catalysts: A review. Appl. Catal. B. 50, 492–531. https://doi.org/10.1016/S0926-3373(98)00040-X

Chen, H., Wei, Z., Kollar, M., Gao, F., Wang, Y., Szanyi, J. (2016). No oxidation on zeolite supported cu catalysts: formation and reactivity of surface nitrates. Catal. Today. 267, 17–27. https://doi.org/10.1016/j.cattod.2015.11.039

Cheng, L., Men, Y., Wang, J., Wang, H., An, W., Wang, Y. (2017). Crystal facet-dependent reactivity of α-Mn_2O_3 microcrystalline catalyst for soot combustion. Appl. Catal., B 204, 374–384.https://doi.org/10.1016/j.apcatb.2016.11.041

Delahay, G., Valade, D., Guzmán-Vargas, A., Coq, B. (2005). Selective catalytic reduction of nitric oxide with ammonia on Fe-ZSM-5 catalysts prepared by different methods. Appl. Catal., B 55, 149–155. https://doi.org/10.1016/j.apcatb.2004.07.009

Du, X., Li, C., Zhao, L., Zhang, J., Lei, G., Sheng, J. (2018). Promotional removal of HCHO from simulated flue gas over Mn-Fe oxides modified activated coke. Appl. Catal., B 232, 37–48. https://doi.org/10.1016/j.apcatb.2018.03.034

Forzatti, P. (2001). Present status and perspectives in de-NO_x SCR catalysis. Appl. Catal., A 222, 221–236. https://doi.org/10.1016/s0926-860x(01)00832-8

Gao, F., Mei, D., Wang, Y., Szanyi, J., Peden, C. (2017). Selective catalytic reduction over Cu/SSZ-13: Linking homo- and heterogeneous catalysis. J. Am. Chem. Soc. 139, 4935–4942. https://doi.org/10.1021/jacs.7b01128

Gee, J.A., Chung, J., Nair, S., Sholl, D.S. (2013). Adsorption and diffusion of small alcohols in zeolitic imidazolate frameworks ZIF-8 and ZIF-90. J. Phys. Chem. C 117, 3169–3176. https://doi.org/10.1021/jp312489w

Guo, X., Li, J., Zhou, R. (2016). Catalytic performance of manganese doped CuO-CeO_2 catalysts for selective oxidation of CO in hydrogen-rich gas. Fuel 163, 56–64. https://doi.org/10.1016/j.fuel.2015.09.043

Han, J., Wang, D., Du, Y., Xi, S., Hong, J., Yin S., Chen, Z., Zhou., T.H. (2015) Metal-organic framework immobilized cobalt oxide nanoparticles for efficient photocatalytic water oxidation. J. Mater. Chem. A 3, 20607–20613. https://doi.org/10.1039/c5ta04675k

Huang, J., Tong, Z., Yan, H., Zhang, J. (2008). Selective catalytic reduction of NO with NH_3 at low temperatures over iron and manganese oxides supported on mesoporous silica. Appl. Catal., B 78, 309–314. https://doi.org/10.1016/j.apcatb.2007.09.031

Huang, X., Lin, Y., Zhang, J., Chen X. (2010). Ligand-directed strategy for zeolite-type metal-organic frameworks: Zinc(II) imidazolates with unusual zeolitic topologies. Angew. Chem. Int. Ed. 45, 1557–1559. https://doi.org/10.1002/anie.200503778

Küsgens, P., Rose, M., Senkovska, I., Fröde, H., Henschel, A., Siegle, S. (2009). Characterization of metal-organic frameworks by water adsorption. Microporous Mesoporous Mater. 120, 325–330. https://doi.org/10.1016/j.micromeso.2008.11.020

Lee, J., Farha, O., Roberts, J., Scheidt, K., Hupp, J. (2009). ChemInform abstract: Metal—organic framework materials as catalysts. ChemInform 40 https://doi.org/10.1002/chin.200933268

Li, C., Tang, X., Yi, H., Wang, L., Cui, X., Chu, C. (2017). Rational design of template-free MnO_x-CeO_2 hollow nanotube as De-NO_x catalyst at low temperature. Appl. Surf. Sci. 428, 924–932. https://doi.org/10.1016/j.apsusc.2017.09.131

Li, D., Yang, G., Li, P., Wang, J., Zhang, P. (2016). Promotion of formaldehyde oxidation over Ag catalyst by Fe doped MnO_x support at room temperature. Cataly. Today. 277, 257–265. https://doi.org/10.1016/j.cattod.2016.02.040

Li, L., Yan, N., Zan, Q., Qiao, S., Yang, S., Guo, Y. (2010). Catalytic oxidation of elemental mercury over the modified catalyst Mn/α-Al_2O_3 at lower temperatures. Environ. Sci. Technol. 44, 426–31. https://doi.org10.1021/es9021206

Liu, S., Wu, X., Duan, W., Min, L., Lee, H.R. (2012). Combined promoting effects of platinum and MnO_x-CeO_2 supported on alumina on NO_x-assisted soot oxidation: thermal stability and sulfur resistance. Chem. Eng. J. 203, 25–35. https://doi.org/10.1016/j.cej.2012.06.090

Lu, Q., Meng, J., Pang, D., Zhang, C., Feng, O. (2015). Reaction and characterization of Co and Ce doped Mn/TiO_2 catalysts for low-temperature SCR of NO with NH_3. Catal. Lett. 2145, 1500–1509. https://doi.org/10.1007/s10562-015-1556-x

Min, K., Park, E.D., Ji, M.K., Yie, J.E. (2007). Manganese oxide catalysts for NO_x reduction with NH_3 at low temperatures. Appl. Catal., A 327, 261–269. https://doi.org/10.1016/j.apcata.2007.05.024

Nguyen, L., Ky, L., Phan, N. (2012). A zeolite imidazolate framework ZIF-8 catalyst for friedel-crafts acylation. Chin. J. Catal. 33, 688–696. https://doi.org/10.1016/S1872-2067(11)60368-9

Niu, Y., Tong, S., Hui, S., Zhang, X., Shui, W. (2016). Synergistic removal of NO and N_2O in low-temperature SCR process with MnO_x/Ti based catalyst doped with Ce and V. Fuel 185, 316–322. https://doi.org/10.1016/j.fuel.2016.07.122

Park, K.S., Ni, Z., Côté, A.P., Choi, J.Y., Huang, R., Uribe-Romo, F.J., Chae, H.K., O'Keeffe, M., Yaghi, O.M. (2006). Exceptional chemical and thermal stability of zeolitic imidazolate frameworks. PNAS 103, 10186–10191. https://doi.org/10.1073/pnas.0602439103

Park, K.H., Sang, M., Kim, S., Dong, W. (2013). Reversibility of Mn valence state in MnO_x/TiO_2 catalysts for low-temperature selective catalytic reduction for no with NH_3. Catal. Lett. 143, 246–253. https://doi.org/10.1007/s10562-012-0952-8

Peng, S., Guo, R.T., Liu, S.M., Wang, S.X., Li, M.Y. (2016). The enhanced performance of MnO_x catalyst for NH_3-SCR reaction by the modification with Eu. Appl. Catal., A 531, 129–138. https://doi.org/10.1016/j.apcata.2016.10.027

Qi, G., Yang, R.T. (2003a). A superior catalyst for low-temperature NO reduction with NH_3. Cheminform 34, 848–849. https://doi.org/10.1039/b212725c

Qi, G., Yang, R.T. (2003b). Performance and kinetics study for low-temperature SCR of NO with NH_3 over MnO_x-CeO_2 catalyst. J. Catal. 217, 434–441. https://doi.org/10.1016/S0021-9517(03)00081-2

Qi, G., Yang, R., Chang, R. (2004). MnO_x-CeO_2 mixed oxides prepared by co-precipitation for selective catalytic reduction of NO with NH_3 at low temperatures. Appl. Catal., B 51, 93–106. https://doi.org/10.1016/j.apcatb.2004.01.023

Qi, G., Yang, R.T., Thompson, L. (2004). Catalytic reduction of nitric oxide with hydrogen and carbon monoxide in the presence of excess oxygen by Pd supported on pillared clays. Appl. Catal., A 259, 261–267. https://doi.org/10.1016/j.apcata.2003.09.040

Shen, Z., Hu, F.Y., Li, J. (2016). Hierarchical core-shell Al_2O_3@Pd-CoAlO microspheres for low-temperature toluene combustion. ACS Catal. 6, 3433–3441. https://doi.org/3433-3441.10.1021/acscatal.6b00144

Singoredjo, L., Korver, R., Kapteijn, F., Moulijn, J. (2010). Alumina supported manganese oxides for the low-temperature selective catalytic reduction of nitric oxide with ammonia. Appl. Catal. B 24, 297–316. https://doi.org/10.1002/chin.199311017

Sun, C., Liu, H., Chen, W., Chen, D., Yu, S., Liu, A. (2018). Insights into the Sm/Zr co-doping effects on N_2 selectivity and SO_2 resistance of a MnO_x-TiO_2 catalyst for the NH_3-SCR reaction. Chem. Eng. J. 347, 27–40. https://doi.org/10.1016/j.cej.2018.04.029

Tran, U.P.N., Le, K.K.N., Phan, N.T.S. (2011). Expanding applications of metal-organic frameworks: zeolite imidazolate framework ZIF-8 as an efficient heterogeneous catalyst for the knoevenagel reaction. ACS Catal. 1, 120–127. https://doi.org/10.1021/cs1000625

Twigg, M.V. (2007). Progress and future challenges in controlling automotive exhaust gas emissions. Appl. Catal., B 70, 2–15. https://doi.org/10.1016/j.apcatb.2006.02.029

Venna, S.R., Jasinski, J.B., Carreon, M.A. (2010). Structural evolution of zeolitic imidazolate framework-8. J. Am. Chem. Soc. 132, 18030. https://doi.org/10.1021/ja109268m

Wang, P., Sun, H., Quan, X., Chen, S. (2016). Enhanced catalytic activity over Mil-100(Fe) loaded ceria catalysts for the selective catalytic reduction of NO_x with NH_3 at low temperature. J. Hazard. Mater. 301, 512–521. https://doi.org/10.1016/j.jhazmat.2015.09.024

Wang, X., Zheng, Y., Lin, J. (2013). Highly dispersed Mn-Ce mixed oxides supported on carbon nanotubes for low-temperature no reduction with NH_3. Catal. Commun. 37, 96–99. https://doi.org/10.1016/j.catcom.2013.03.035

Wei, Y., Chen, Y., Wang, R. (2018). Rare earth salt of 12-tungstophosphoric acid supported on iron oxide as a catalyst for selective catalytic reduction of NO_x. Fuel Process. Technol. 178, 262–270. https://doi.org/10.1016/j.fuproc.2018.06.001

Wu, Z., Jiang, B., Liu, Y., Zhao, W., Guan, B. (2007). Experimental study on a low-temperature SCR catalyst based on MnO_x/TiO_2 prepared by sol-gel method. J. Hazard. Mater. 145, 488–494. https://doi.org/10.1016/j.jhazmat.2006.11.045

Yang, S., Qi, F., Xiong, S., Hao, D., Li, J. (2016). MnO_x supported on Fe-Ti spinel: A novel Mn based low temperature SCR catalyst with a high N_2 selectivity. Appl. Catal., B 181, 570–580. https://doi.org/10.1016/j.apcatb.2015.08.023

Yi, L., Zheng, L., Mnichowicz, B., Harinath, A., Li, H., Bahrami, B. (2016). Chemical deactivation of commercial vanadium SCR catalysts in diesel emission control application. Chem. Eng. J. 287, 680–690. https://doi.org/10.1016/j.cej.2015.11.043

Yu, J., Guo F., Wang, Y., Zhu, J., Liu, Y., Su, F., Gao, S., Xu, G. (2010). Sulfur poisoning resistant mesoporous Mn-base catalyst for low-temperature SCR of NO with NH_3. Appl. Catal., B 95, 160–168. https://doi.org/10.1016/j.apcatb.2009.12.023

Zhang, L., Shi, L., Huang, L., Zhang, J., Ga, R., Zhang, D. (2014). Rational design of high-performance $DeNO_x$ catalysts based on $Mn_xCo_{3-x}O_4$ nanocages derived from metal-organic frameworks. ACS Catal. 4, 1753−1763. https://doi.org/10.1021/cs401185c

Zhang, S., Zhao, Y., Yang, J., Zhang, J., Zheng, C. (2018). Fe-modified MnO_x/TiO_2 as the SCR catalyst for simultaneous removal of NO and mercury from coal combustion flue gas. Chem. Eng. J. 348, 618–629. https://doi.org/10.1016/j.cej.2018.05.037

Zhang, W., Shi, Y., Li, C., Zhao, Q., Li, X. (2016). Synthesis of bimetallic MOFs MIL-100(Fe-Mn) as an efficient catalyst for selective catalytic reduction of NO_x with NH_3. Catal. Lett. 146, 1956–1964. https://doi.org/10.1007/s10562-016-1840-4

Zhang, X., Shen, B., Zhang, X., Wang, F., Chi, G., Si, M. (2017). A comparative study of manganese-cerium doped metal-organic frameworks prepared via impregnation and in situ methods in the selective catalytic reduction of NO. RSC Adv. 7, 5928–5936. https://doi.org/10.1039/c6ra25413f

Zhao, L., Li, C., Li, S.,Wang, Y., Zhang, J., Wang, T., Zeng, G. (2016). Simultaneous removal of elemental mercury and NO in simulated flue gas over V_2O_5/ZrO_2-CeO_2 catalyst. Appl. Catal., B 198, 420–430. https://doi.org/10.1016/j.apcatb.2016.05.079